ON SAMPLING-BIORTHOGONAL TIME-DOMAIN SCHEME BASED ON DAUBECHIES COMPACTLY SUPPORTED WAVELETS

Y. Tretiakov

IBM Microelectronics
Essex Junction, VT 05452, USA

S. Ogurtsov and G. Pan

Department of Electrical Engineering
Arizona State University
Tempe, AZ 85287, USA

Abstract—The multi-resolution time domain (MRTD) technique for electromagnetic field equations was proposed by Krumpholz, Katehi *et al.*, using Battle-Lemarie wavelets. The basis principle behind the MRTD is the wavelet-Galerkin time domain (WGTD) approach. Despite its effectiveness in space discretization, the complexity of the MRTD makes it unpopular. Recently, the WGTD was significantly simplified by Cheong *et al.* based on the approximate sampling property of the shifted versions of the Daubechies compactly supported wavelets. In this paper, we provide a rigorous analysis of the MRTD, employing positive sampling functions and their biorthogonal dual. We call our approach as the sampling biorthogonal time-domain (SBTD) technique. The introduced sampling and dual functions are both originated from Daubechies scaling functions of order 2 (referred as to D_2), and form a biorthonormal system. This biorthonormal system has exact interpolation properties and demonstrates superiority over the FDTD in terms of memory and speed. Numerical examples and comparisons with the traditional FDTD results are provided.

1. INTRODUCTION

The multiresolution time domain (MRTD) technique was proposed in
[1] for the solution of Maxwell's equations, in which the electrical and
magnetic field components are expanded with pulse basis in time and
Battle-Lemarie wavelets in space. It was shown that the standard
FDTD is equivalent to the Galerkin method with Haar wavelets,
i.e., piecewise constants with discontinuities at the edges [1]. The
Battle-Lemarie wavelets, on the other hand, are continuous functions,
thus offering better convergence rates. In the MRTD, the standard
Galerkin procedure converts the two vector curl equations into a system
consisting of six updating equations similar to the traditional FDTD
scheme of Yee [2]. For instance, one of the six equations is

$$
\begin{aligned}
{}_{k+1}E^x_{l+1/2,m,n} ={} & {}_k E^x_{l+1/2,m,n} \\
& + \frac{\Delta t}{\varepsilon_{l+1/2,m,n}} \left[\frac{1}{\Delta y} \sum_{i=-L_s}^{L_s-1} a_i \cdot {}_{k+1/2}H^z_{l+1/2,m+i+1/2,n} \right.\\
& \left. - \frac{1}{\Delta z} \sum_{i=-L_s}^{L_s-1} a_i \cdot {}_{k+1/2}H^y_{l+1/2,m,n+i+1/2} \right]
\end{aligned}
\tag{1}
$$

where L_s denotes the effective support size of the basis function $\phi(x)$.
The other five updating equations of the MRTD scheme are derived in
the same manner.

In the MRTD, the unknown functions are expanded in terms
of basis functions, which are the Battle-Lemarie scaling functions

or wavelets. The coefficient $\{a_i\}$, representing the weight of the contributions to a node by its neighbors, must be pre-computed. For $i \geq 0$, $\{a_i\}$ are calculated numerically as

$$a_i = \int_{-\infty}^{+\infty} \phi_{-i}(x) \frac{\partial \phi_{1/2}(x)}{\partial x} dx. \tag{2}$$

For $i < 0$ the coefficients $\{a_i\}$ are given by the symmetry relation

$$a_i = -a_{-1-i}. \tag{3}$$

It has been found numerically [1] that for the Battle-Lemarie wavelets coefficients $\{a_i\}$ for $i \geq 9$ and $i \leq -10$ are negligible, that is $L_s \approx 9$.

It was reported in [1] that for a cubic resonator problem the MRTD algorithm reduces memory size by 125, yet providing the same accuracy as the traditional FDTD does. Despite its efficiency in discretization, the complexity in the expressions and programming has overweighted the advantage of using wavelets in the MRTD. For instance, in the FDTD, a simple finite difference equation consists of six terms, representing a particular node and its direct neighbors. In contrast, in the MRTD the same finite difference equation comprises of 20 terms, involving the immediate, secondary, and up to nine neighbors, due to the non-compact support of the wavelets. In the mean time, the field quantity at a node equals the summation of the particular values at all related neighboring points. Such a distribution nature makes the MRTD very inconvenient for implementation of radiation or absorption boundary conditions.

To improve the effectiveness of the MRTD, the Wavelet-Galerkin time-domain (WGTD) scheme was proposed by Cheong *et al* [3], employing Daubechies compactly supported wavelets of D_2 [4]. The basic idea behind WGTD is the same as that in the MRTD [1], but the WGTD has the advantage of short expressions because the Daubechies wavelets have finite supports. In addition, the sampling property gets rid of the distribution nature of the solution, i.e., the field value at a particular node is uniquely related to the expansion coefficient at that node.

In this paper the positive sampling basis and its biorthogonal dual testing functions are constructed, employing the Daubechies scaling functions D_2. Owing to the exact sampling property of the basis functions and their biorthogonal testing functions, the expansion and testing procedures are both rigorous for the sampling-biorthogonal time-domain (SBTD) method. The approximation is only in the numerical evaluation of the coefficients of a_i, which involve the integral of Daubechies ϕ_{-i} multiplied by a derivative of a staggered Daubechies. As a result, the error estimate can be easily conducted.
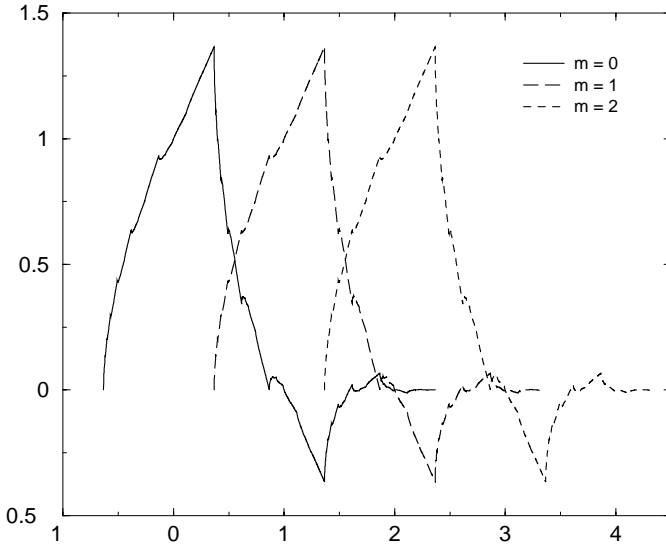
Figure 1. Daubechies shifted scaling functions ($N = 2$) for $m = 0, 1, 2$.

2. WGTD SCHEME BASED UPON SHIFTED DAUBECHIES D_2 SCALING FUNCTIONS

It was remarked by mathematicians [5], that shifted Daubechies D_2 scaling functions have approximate sampling properties, namely

$$\phi(k + M_1) \approx \delta_{k,0} \tag{4}$$

where $M_1 = \int_{-\infty}^{+\infty} x\phi(x)dx$. For Daubechies scaling functions of order $N = 2$, referred to as D_2, the support is $[0, 3]$. $M_1 = (1 + \sqrt{3})/4 \approx 0.683$, $\phi(M_1) \approx 1.00020859077$, $\phi(M_1 + 1) \approx -4.17181539384E - 04$, and $\phi(M_1 + 2) \approx 2.08590769692E - 04$. Interestingly enough, D_2 is similar to the Shannon sampling functions of $\sin(\pi n)/(\pi n) = \delta_{n,0}$, but the latter has an infinite support.

Cheong *et al.* immediately recognized these approximate sampling properties, and developed the Wavelet-Galerkin time domain (WGTD) algorithm [3]. To make use of the shifted interpolation property (4) we recall the following expansion functions

$$\phi_m(x) = \phi\left(\frac{x}{\Delta x} - m + M_1\right). \tag{5}$$

Plotted in Fig. 1 are functions defined in (5) with $\Delta x = 1$ and

$m = 0, 1, 2$. Due to finite support of Daubechies scaling functions, the number of nonzero coefficients $\{a_i\}$ is also finite. One can easily verify that $a_i \neq 0$ for $-3 \leq i \leq 2$ and hence $L_s = 3$ in (1). The numerical values of the coefficients $\{a_i\}$ have been tabulated in [3].

From the above discussion it follows that the use of Daubechies scaling functions is more computationally efficient than that of the Battle-Lemarie scaling functions. A more profound advantage of the WGTD is the sampling property (4). It follows that the total field at any space point is equal to the corresponding expansion coefficient at that point, namely

$$E_x(l\Delta x, m\Delta y, n\Delta z, k\Delta t) = {}_k E^x_{l+1/2,m,n}.$$ (6)

This sampling property has eliminated the distribution nature of the MRTD method. As a result, boundary conditions can easily be incorporated.

3. THE SBTD SCHEME BASED ON BIORTHOGONAL SAMPLING BASIS

To construct the Daubechies based biorthogonal sampling basis we use the following expression in [6] for a positive sampling function

$$S(x) = \frac{2\nu}{\nu - 1} \sum_{n=0}^{+\infty} \left(\frac{1+\nu}{1-\nu} \right)^n \phi(x - n + 1),$$ (7)

where $\phi(x)$ is the Daubechies scaling function, not necessary just D_2. However, in rest of the paper we shall restrict the Daubechies scaling functions to only D_2. The parameter ν is equal to $-1/\sqrt{3}$. We notice here that $\phi(1) = \frac{\nu-1}{2\nu}$, $\phi(2) = \frac{\nu+1}{2\nu}$ (see [4] for details) and thus we may rewrite (7) in the form

$$S(x) = \frac{1}{\phi(1)} \sum_{n=0}^{+\infty} \left(\frac{|\phi(2)|}{\phi(1)} \right)^n \phi(x - n + 1).$$ (8)

We define the shifted versions of the sampling function $S(x)$ as

$$S_m(x) = S(x - m).$$ (9)

The following exact interpolating property holds for the above-defined sampling function $S_m(x)$

$$S_m(k) = \delta_{m,k}.$$ (10)

The proof can be found in Appendix. The support of the sampling function $S_m(x)$ is $[m-1, +\infty)$. Notice that a sampling function $\{S_m(x)\}$ is not orthogonal with respect to its shift

$$\int_{-\infty}^{+\infty} S_m(x) S_n(x) dx \neq \delta_{m,n}. \tag{11}$$

Therefore the biorthogonal testing functions $Q_n(x)$ were introduced in [6], such that

$$Q_n(x) = \sum_p \phi(x-p)\phi(n-p) \tag{12}$$

It was shown that $\{Q_n(x)\}$ is a Riesz basis, biorthogonal to $\{S_m(x)\}$, namely

$$\int_{-\infty}^{+\infty} Q_n(x) S_m(x) dx = \delta_{n,m}. \tag{13}$$

We checked the above biorthogonality for the case when we use the Daubechies scaling functions D_2 as a function $\phi(x)$. The detailed analytical derivations can be found in Appendix. Due to the finite support of the Daubechies scaling functions we simplify expression (12) to the following compact form

$$Q_n(x) = \phi(x-n+2)\phi(2) + \phi(x-n+1)\phi(1). \tag{14}$$

From (14) it follows immediately that $Q_n(x)$ is supported on $[n-2, n+2]$. The sampling function $S(x) = S_0(x)$ and biorthogonal function $Q(x) = Q_0(x)$ are plotted in Fig. 2.

For the SBTD scheme we use the following basis for expansion

$$s_m(x) = S\left(\frac{x}{\Delta x} - m\right) \tag{15}$$

and the biorthogonal testing functions

$$q_n(x) = Q\left(\frac{x}{\Delta x} - n\right). \tag{16}$$

After applying the standard expansion and testing procedures, the two vector curl Maxwell equations become six updating expressions, analogous to (1) with coefficients $\{a_i\}$ given by

$$a_i = \int_{-\infty}^{+\infty} Q_{-i}(x) \frac{\partial S_{1/2}(x)}{\partial x} dx. \tag{17}$$

Due to rapid decay of the sampling function $S(x)$ and finite support of the testing function $Q(x)$, the number of the nonzero
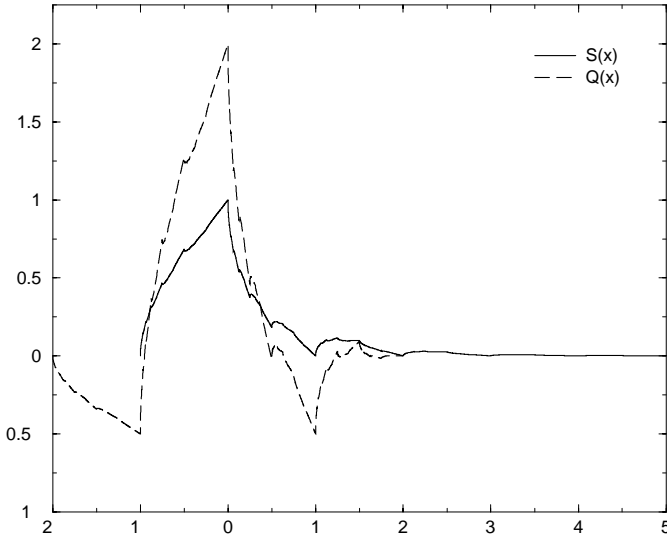
Figure 2. Sampling function $S(x)$ and biorthogonal function $Q(x)$.

coefficients $\{a_i\}$ is small, as in the case of WGTD technique with the shifted Daubechies basis. In fact, we obtained from (17) that for $i \geq 3$ all coefficients $\{a_i\}$ are exactly zeros. This is due to the specific supports of the functions $S(x)$ and $Q(x)$. It has been found analytically that for $i \leq -4$ all coefficients $\{a_i\}$ in (17) are also exactly zeros. One can find in Appendix the derivation for $i = -4$. For $-3 \leq i \leq 2$ the following identity is true

$$\int_{-\infty}^{+\infty} Q_{-i}(x) \frac{\partial S_{1/2}(x)}{\partial x} dx = \int_{-\infty}^{+\infty} \phi_{-i}(x) \frac{\partial \phi_{1/2}(x)}{\partial x} dx. \qquad (18)$$

This means that $L_s = 3$ and $\{a_i\}$ are exactly the same as in [3]. In Appendix we presented analytical verification of the identity (18) for $i = 1$.

   We conclude that the numerical results will be exactly the same for technique in the previous section and technique in this section, although the sampling function $S_m(x)$ obeys the exact interpolation property (10). The advantage of using the biorthogonal sampling system is that the error introduced in the truncation process can be explicitly identified. Hence, the error bound can be estimated easily. In contrast, for the shifted Daubechies WGTD, the errors are inexplicitly reflected by the numerical values of the D_2 scaling functions. As mathematicians pointed out that no one knows the exact value of $\phi(\sqrt{2})$, nor $\phi(1 + \sqrt{3})/4$.

4. FORMULATION AND BOUNDARY CONDITIONS FOR THE SBTD TECHNIQUE

The SBTD scheme based on constructed in the previous section biorthogonal sampling basis has the following six updating equations

$$_{k+1/2}H^x_{l,m+1/2,n+1/2} = {}_{k-1/2}H^x_{l,m+1/2,n+1/2}$$

$$+\frac{\Delta t}{\mu_{l,m+1/2,n+1/2}}\left[\frac{1}{\Delta z}\sum_{i=-3}^{2}a_i\cdot{}_kE^y_{l,m+1/2,n+i+1}\right.$$

$$\left.-\frac{1}{\Delta y}\sum_{i=-3}^{2}a_i\cdot{}_kE^z_{l,m+i+1,n}\right] \qquad (19)$$

$$_{k+1/2}H^y_{l+1/2,m,n+1/2} = {}_{k-1/2}H^y_{l+1/2,m,n+1/2}$$

$$+\frac{\Delta t}{\mu_{l+1/2,m,n+1/2}}\left[\frac{1}{\Delta x}\sum_{i=-3}^{2}a_i\cdot{}_kE^z_{l+i+1,m+1/2,n}\right.$$

$$\left.-\frac{1}{\Delta z}\sum_{i=-3}^{2}a_i\cdot{}_kE^x_{l+1/2,m,n+i+1}\right] \qquad (20)$$

$$_{k+1/2}H^z_{l+1/2,m+1/2,n} = {}_{k-1/2}H^z_{l+1/2,m+1/2,n}$$

$$+\frac{\Delta t}{\mu_{l+1/2,m+1/2,n}}\left[\frac{1}{\Delta y}\sum_{i=-3}^{2}a_i\cdot{}_kE^x_{l+1/2,m+1+i,n}\right.$$

$$\left.-\frac{1}{\Delta x}\sum_{i=-3}^{2}a_i\cdot{}_kE^y_{l+1+i,m+1/2,n}\right] \qquad (21)$$

$$_{k+1}E^x_{l+1/2,m,n} = {}_kE^x_{l+1/2,m,n}$$

$$+\frac{\Delta t}{\varepsilon_{l+1/2,m,n}}\left[\frac{1}{\Delta y}\sum_{i=-3}^{2}a_i\cdot{}_{k+1/2}H^z_{l+1/2,m+i+1/2,n}\right.$$

$$\left.-\frac{1}{\Delta z}\sum_{i=-3}^{2}a_i\cdot{}_{k+1/2}H^y_{l+1/2,m,n+i+1/2}\right] \qquad (22)$$

$$_{k+1}E^y_{l,m+1/2,n} = {}_kE^y_{l,m+1/2,n}$$

$$+\frac{\Delta t}{\varepsilon_{l,m+1/2,n}}\left[\frac{1}{\Delta z}\sum_{i=-3}^{2}a_i\cdot{}_{k+1/2}H^x_{l,m+1/2,n+1/2+i}\right.$$

$$-\frac{1}{\Delta x}\sum_{i=-3}^{2} a_i \cdot {}_{k+1/2}H^z_{l+1/2+i,m+1/2,n}\Bigg] \qquad (23)$$

$${}_{k+1}E^z_{l,m,n+1/2} = {}_kE^z_{l,m,n+1/2}$$

$$+\frac{\Delta t}{\varepsilon_{l,m,n+1/2}}\Bigg[\frac{1}{\Delta x}\sum_{i=-3}^{2} a_i \cdot {}_{k+1/2}H^y_{l+1/2+i,m,n+1/2}$$

$$-\frac{1}{\Delta y}\sum_{i=-3}^{2} a_i \cdot {}_{k+1/2}H^x_{l,m+1/2+i,n+1/2}\Bigg] \qquad (24)$$

If the structure under investigation is terminated by a perfect electric conductor (PEC) then boundary conditions are modeled using the image theory. In that situation property (6) is very important and facilitates boundary condition implementation.

As an excitation field we use Gaussian pulse

$$f(t) = A_0 \cdot exp\left[-\left(\frac{t-t_0}{T}\right)^2\right] \qquad (25)$$

and force an electric field coefficient at some particular node inside the computation domain to be equal $f(t)$ during the excitation time.

5. NUMERICAL RESULTS

To validate the newly implemented biorthogonal sampling basis we include a few numerical examples.

Example 1. Eigenfrequency problem.

A 2D parallel plate resonator is depicted in Fig. 3. For the sake of simplicity we analyze only the polarization for which $E_x = 0$, $E_y = 0$ and $H_z = 0$. The dimensions are $a = 2$ m, $b = 1$ m and the time step $\Delta t = 10^{-10}$ sec. The electric field values E_z were sampled during the time period $T_s = 2^{16}\Delta t$ and the fast Fourier transform (FFT) was performed to obtain the spectrum of the sampled field E_z. Illustrated in Fig. 3 are the numerical results obtained with $15 \times 7 = 105$ Yee cells for both FDTD and SBTD techniques, along with analytical values. It can be seen clearly that SBTD provides better agreement with the analytical solution, though it is slower than the FDTD approach. The computational time is 8.93 sec for FDTD method and 39.89 sec for SBTD.

To achieve the SBTD accuracy, we decreased the size of the cell in the FDTD. As a result, $40 \times 20 = 800$ Yee cells for FDTD demonstrated
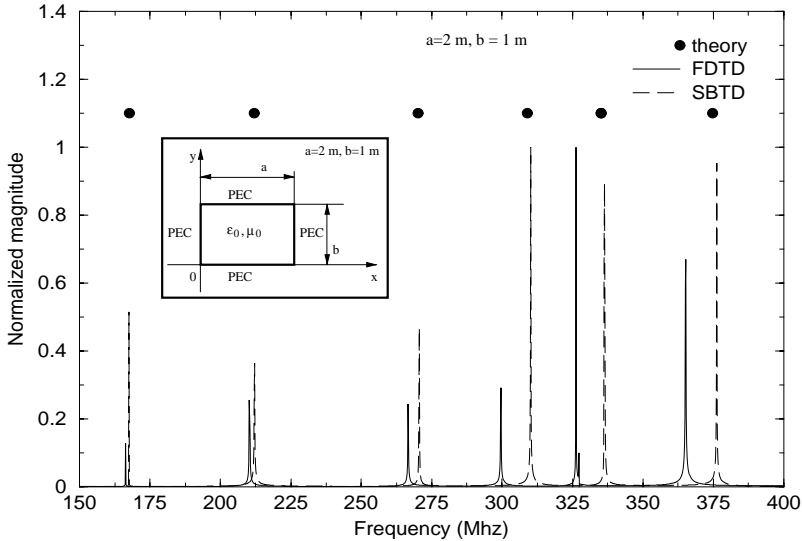
Figure 3. Magnitude of the electric field component E_z in the frequency domain (air-filled 2D resonator).

the precision of the SBTD with 105 cells. The results are shown in Fig. 4. The computational time for the FDTD increased to 66.36 sec due to increased number of Yee cells. As can be seen in the figure, both methods give almost the same results for the eigenfrequency, but the SBTD approach here is more efficient in terms of computational time and computer memory.

Example 2. Partially loaded 2D resonator.

Here we consider the previous resonator, but filled in part with a dielectric slab, as shown in Fig. 5. The additional parameters are $h = 0.2$ m and $\varepsilon_r = 2.0$. We use the same number of Yee cells for the SBTD and FDTD, namely $20 \times 10 = 200$. From Fig. 5, it can be seen again that the SBTD technique gives better prediction of the resonance frequencies than the standard Yee's FDTD approach.

Example 3. Air-filled 3D cavity.

The air-filled 3D cavity is shown in Fig. 6. The parameters used in numerical computations are $a = 1.2$ m, $b = 0.6$ m, $c = 0.8$ m. The time step was $\Delta t = 0.8 \cdot 10^{-10}$ sec. The three electric field components were sampled during the time period $T_s = 2^{16}\Delta t$ and FFT was performed to obtain the frequency spectrum of the sampled electric field.

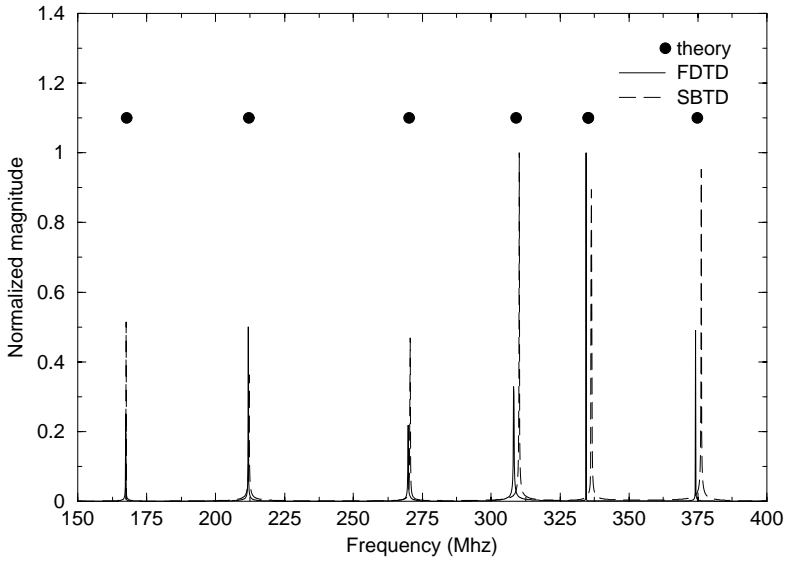Shown in Fig. 6 are the numerical results obtained with $6 \times 3 \times$

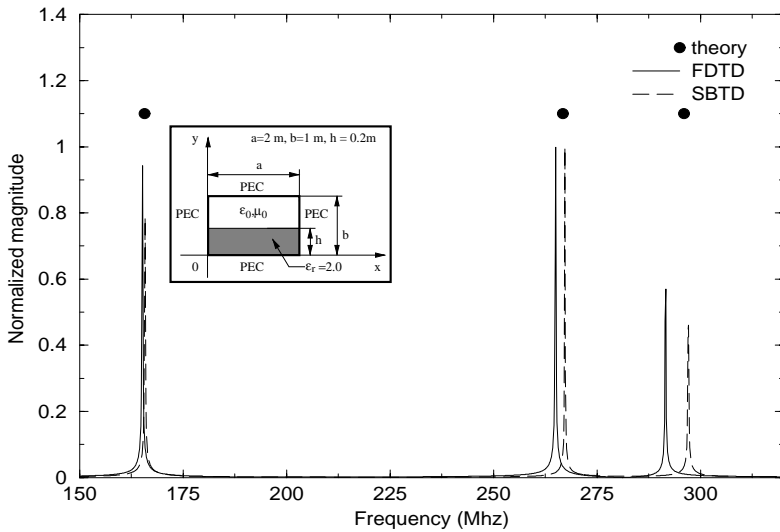**Figure 4.** Magnitude of the electric field component E_z in the frequency domain (air-filled 2D resonator).

Figure 5. Magnitude of the electric field component E_z in the frequency domain (partially filled with dielectric 2D resonator).
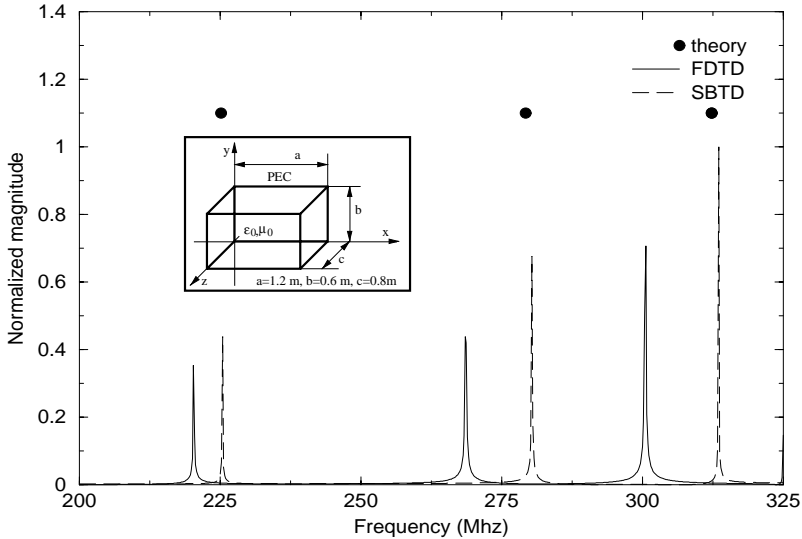
Figure 6. Magnitude of the electric field in the frequency domain (air-filled 3D cavity).

$4 = 72$ Yee cells for both FDTD and SBTD techniques, along with analytical values. One can see that SBTD has better agreement with the theoretical results, though it is more computationally expensive than FDTD. Namely, the computational time is 23.8 sec for FDTD method and 125.7 sec for SBTD.

To achieve also a good accuracy for FDTD technique, we increased the number of Yee cells. The numerical results are shown in Fig. 7 where FDTD has $24 \times 12 \times 16 = 4608$ cells and SBTD - 72. The computational time for FDTD increased to 1608.9 sec It is obvious that SBTD approach here is more efficient in terms of computational time and computer memory. To be more specific, we need $4608/72 = 64$ times less computer memory for SBTD method than for FDTD approach to get an accurate result. At the same time SBTD technique will be also $1608.9/125.7 \approx 13$ times faster than FDTD.

Table 1 also summarizes numerical results in terms of the lowest resonance frequency (TE_{101} mode), mesh size, computational time and numerical error. Time is given in sec, error in % and the resonance frequency in Mhz. Theoretical value of the lowest resonance frequency for the given in this example parameters is 225.191 Mhz.

Example 4. Partially filled 3D cavity.

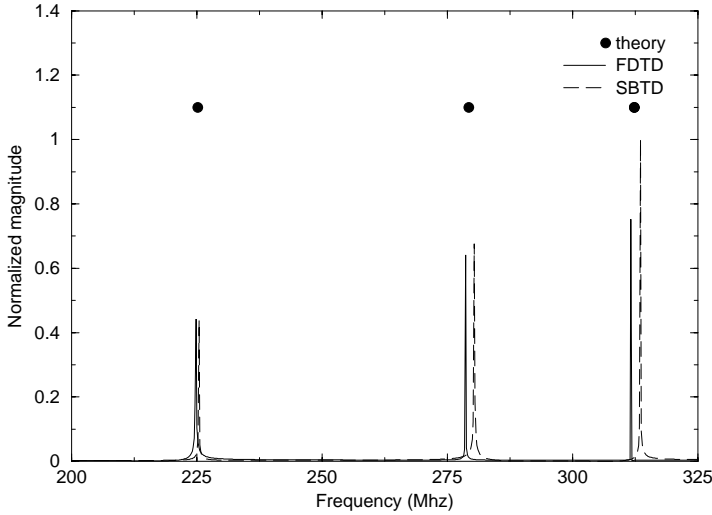The partially filled with the dielectric 3D cavity is shown in Fig. 8.

Figure 7. Magnitude of the electric field in the frequency domain (air-filled 3D cavity).

Table 1. Lowest resonance frequency (air-filled 3D cavity).

Mesh	FDTD			SBTD		
	Frequency	Error	Time	Frequency	Error	Time
$6 \times 3 \times 4$	220.299	2.17251	23.8	225.449	0.11437	125.7
$12 \times 6 \times 8$	223.923	0.56322	193.9	N/A	N/A	N/A
$24 \times 12 \times 16$	224.876	0.13972	1608.9	N/A	N/A	N/A

The parameters are $a = 1.2\,\text{m}$, $b = 0.6\,\text{m}$, $c = 0.8\,\text{m}$, $h = 0.3\,\text{m}$ and $\varepsilon_r = 2.0$.

Table 2 shows numerical results in terms of the lowest resonance frequency (hybrid TE_{10}^y mode), mesh size, computational time and numerical error. Time is given in sec, error in % and the resonance frequency in Mhz. Theoretical value of the lowest resonance frequency is 224.364 Mhz.

We can see that for the mesh with $6 \times 4 \times 4 = 96$ cell SBTD is more accurate than FDTD method. If we increase number of Yee cells for FDTD technique then we get a more accurate results. This can be clearly seen from the Table 2. In that case FDTD computation time will also increase. If we compare the results obtained by using FDTD with $12 \times 8 \times 8 = 768$ cell then we see that accuracy is less than 1 %. but in that case we need $768/96 = 8$ times more computer
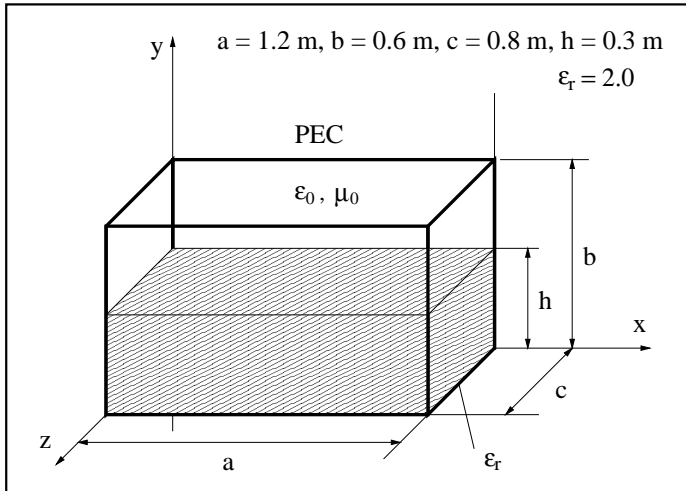
Figure 8. Partially filled 3D cavity.

Table 2. Lowest resonance frequency (partially filled 3D cavity).

Mesh	FDTD			SBTD		
	Frequency	Error	Time	Frequency	Error	Time
$6 \times 4 \times 4$	219.272	2.06684	31.2	225.83	0.65352	168.8
$12 \times 8 \times 8$	223.161	0.53618	255.4	N/A	N/A	N/A
$24 \times 16 \times 16$	223.923	0.19656	2119.5	N/A	N/A	N/A

memory than for SBTD technique. FDTD is also $255.4/168.8 \approx 1.5$ times slower than SBTD.

Example 5. Waveguide problem.

As an example of a waveguide problem, we model an air-field rectangular waveguide using the technique described in [7]. The cross-sectional dimensions are $a = 2\,\mathrm{m}$, $b = 1\,\mathrm{m}$. In Fig. 9 we plotted the normalized propagation constant β_z/k_0 versus frequency for a few eigenmodes, starting with the dominant mode TE_{10}^z. To verify our numerical SBTD results we also plotted the dispersion curves from theoretical formulation and from FDTD.

For SBTD method we used mesh with $20 \times 10 = 200$ cells. To reach a competitive precision, the FDTD mesh requires $44 \times 22 = 968$ cells. For each particular value of β_z the computational time was approximately equal to 150 seconds for SBTD and 204 seconds for FDTD.
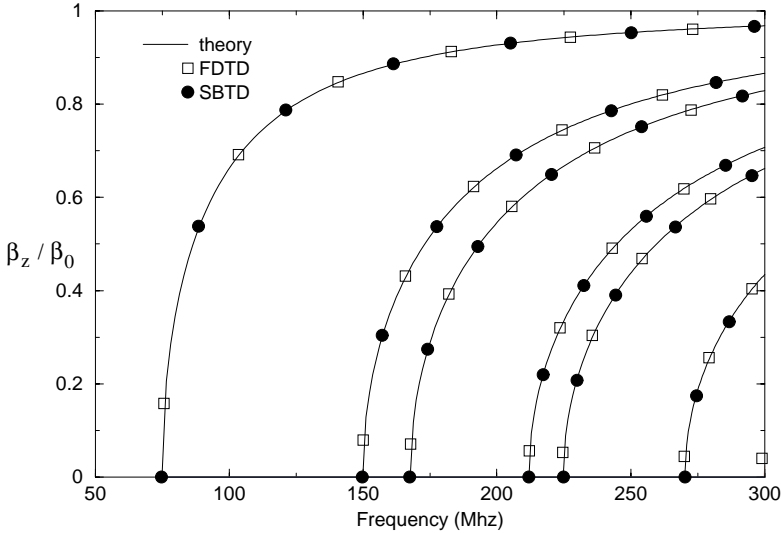
Figure 9. Normalized propagation constant β_z/k_0 versus frequency (Hz).
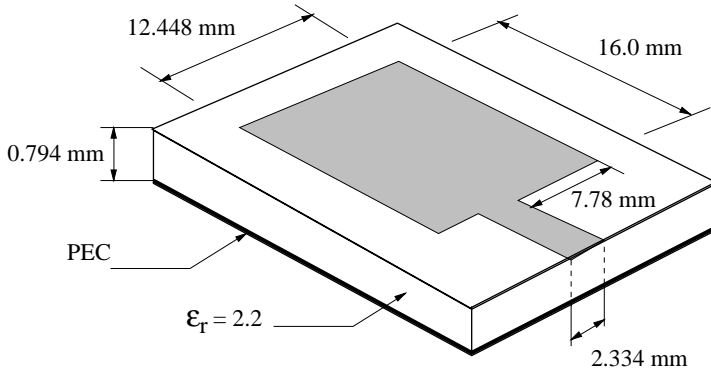

Figure 10. Rectangular patch antenna.

Example 6. Rectangular patch antenna.

In the last numerical example we analyze the rectangular microstrip patch antenna, shown in Fig. 10. This structure has been previously analyzed in [8].

For the reference solution we used FDTD with the following space steps: $\Delta x = 0.8120\,\mathrm{mm}$, $\Delta y = 0.8120\,\mathrm{mm}$, and $\Delta z = 0.3970\,\mathrm{mm}$. The mesh size was $60 \times 100 \times 16 = 96000$ cells and the time step $0.441\,\mathrm{ps}$.

For the SBTD technique we implemented mesh with $30 \times 50 \times 8 = 12000$ cells. We also used smaller mesh size for the FDTD technique. The results in terms of scattering parameter $|S_{11}|$ are shown in Fig. 11. The computation time for the most accurate solution is 4739.2 seconds. For the SBTD approach the CPU time is 2760.8 seconds.
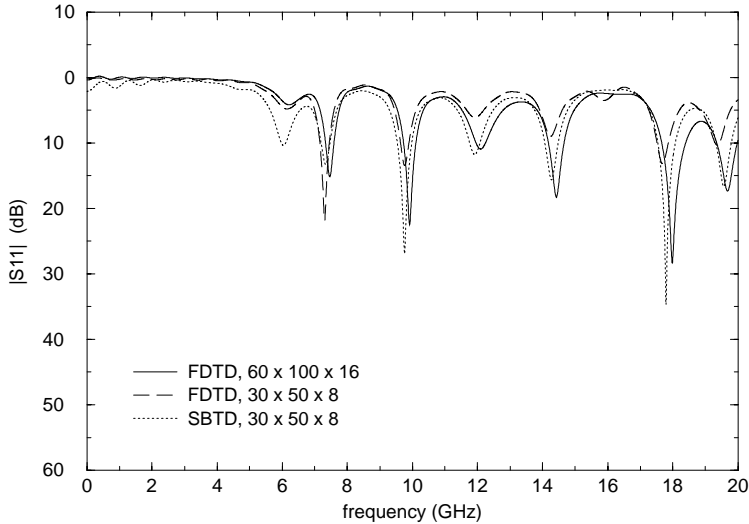

Figure 11. Return loss of the rectangular patch antenna.

To close the open microwave patch antenna structure in the FDTD and SBTD techniques, the PML absorbing boundary conditions [9] are used.

As we can see from Fig. 11 the SBTD technique gives still good result for the smaller mesh size than FDTD. It means, that we can use SBTD with a smaller mesh still having an accurate result. For the results presented in Fig. 11, the SBTD method gives factors of 8 and $4739.2/2760.8 \approx 1.7$ of the computer memory and computational time savings, respectively.

6. CONCLUSION

The Sampling-Biorthogonal Time-Domain scheme is derived based biorthogonal sampling system of the Daubechies D_2 scaling functions. The exact interpolation property of the basis functions, the rapid decay and finite support of the testing functions lead to simplified forms of the updating equations. The newly implemented SBTD technique demonstrated better efficiency in terms of accuracy,

computational time and computer memory than the traditional FDTD and previously developed MRTD technique. The new algorithm was tested numerically with a number of examples and showed accurate results and good efficiency.

APPENDIX A.

First we show that the following exact interpolation property holds for the defined above sampling function $S_m(x)$

$$S_m(k) = \delta_{m,k}. \tag{A1}$$

From the definition of $S_m(x)$ we have

$$S_m(k) = \frac{1}{\phi(1)} \sum_{n=0}^{+\infty} \left(\frac{|\phi(2)|}{\phi(1)} \right)^n \phi(k - m - n + 1). \tag{A2}$$

In the above equation only two terms are non zero due to the finite support of the scaling function $\phi(x)$, namely $\phi(1) \neq 0$ and $\phi(2) \neq 0$. It means that $k - m - n + 1 = 1, 2$ or $n = k - m - 1, k - m$. Therefore equation (A2) can be rewritten in the form

$$S_m(k) = \frac{1}{\phi(1)} \left[\left(\frac{|\phi(2)|}{\phi(1)} \right)^{k-m-1} \phi(2) + \left(\frac{|\phi(2)|}{\phi(1)} \right)^{k-m} \phi(1) \right]. \tag{A3}$$

If $k = m$ then $n = k - m - 1 = -1$ and we don't have the first term in (A3) since the summation in (A2) starts from $n = 0$. This gives us the following

$$S_m(m) = \frac{1}{\phi(1)} \left(\frac{|\phi(2)|}{\phi(1)} \right)^0 \phi(1) = 1. \tag{A4}$$

If $k \neq m$ then by using the fact that $\phi(2)$ is negative we get the following

$$S_m(k) = \frac{1}{\phi(1)} \left[-\frac{|\phi(2)|^{k-m}}{\phi(1)^{k-m-1}} + \frac{|\phi(2)|^{k-m}}{\phi(1)^{k-m-1}} \right] = 0. \tag{A5}$$

The biorthogonality property (13) can be checked very easily in the following way. First we have

$$\int_{-\infty}^{+\infty} Q_n(x) S_m(x) dx = \frac{1}{\phi(1)} \sum_{p=0}^{+\infty} \left(\frac{|\phi(2)|}{\phi(1)} \right)^p$$

$$\cdot \int_{-\infty}^{+\infty} (\phi(x-n+2)\phi(2) + \phi(x-n+1)\phi(1))$$

$$\cdot \phi(x-m-p+1)dx. \tag{A6}$$

If we use the orthogonality of Daubechies' scaling functions $\{\phi(x)\}$, then the above expression becomes

$$\int_{-\infty}^{+\infty} Q_n(x)S_m(x)dx = \frac{1}{\phi(1)}\left[\left(\frac{|\phi(2)|}{\phi(1)}\right)^{n-m-1}\phi(2) + \left(\frac{|\phi(2)|}{\phi(1)}\right)^{n-m}\phi(1)\right]. \tag{A7}$$

Again, if $m = n$ then we don't have a first term in (A7) and hence

$$\int_{-\infty}^{+\infty} Q_n(x)S_m(x)dx = \frac{1}{\phi(1)}\left(\frac{|\phi(2)|}{\phi(1)}\right)^0 \phi(1) = 1. \tag{A8}$$

If $m \neq n$ then we have

$$\int_{-\infty}^{+\infty} Q_n(x)S_m(x)dx = \frac{1}{\phi(1)}\left[-\frac{|\phi(2)|^{n-m}}{\phi(1)^{n-m-1}} + \frac{|\phi(2)|^{n-m}}{\phi(1)^{n-m-1}}\right] = 0. \tag{A9}$$

To verify that $a_{-4} = 0$ again we use the definition of the functions $S_m(x)$ and $Q_n(x)$. We have the following

$$a_{-4} = \int_{-\infty}^{+\infty} Q_4(x)\frac{\partial S_{1/2}(x)}{\partial x}dx = \frac{1}{\phi(1)}\sum_{p=0}^{+\infty}\left(\frac{|\phi(2)|}{\phi(1)}\right)^p$$

$$\cdot \int_{-\infty}^{+\infty} [\phi(x-2)\phi(2) + \phi(x-3)\phi(1)]\frac{\partial \phi_{p-1/2}(x)}{\partial x}dx. \tag{A10}$$

The finite support $[0,3]$ of the Daubechies' scaling function $\phi(x)$ with $N = 2$ gives rise to the following

$$a_1 = \frac{1}{\phi(1)}[I_1 + I_2], \tag{A11}$$

with I_1 given by

$$\begin{aligned}
I_1 &= -|\phi(2)|\int_{-\infty}^{+\infty}\phi(x-2)\frac{\partial\phi(x+1/2)}{\partial x}dx \\
&\quad -\frac{|\phi(2)|^2}{\phi(1)}\int_{-\infty}^{+\infty}\phi(x-2)\frac{\partial\phi(x-1/2)}{\partial x}dx \\
&\quad -\frac{|\phi(2)|^3}{(\phi(1))^2}\int_{-\infty}^{+\infty}\phi(x-2)\frac{\partial\phi(x-3/2)}{\partial x}dx
\end{aligned}$$

$$-\frac{|\phi(2)|^4}{(\phi(1))^3} \int_{-\infty}^{+\infty} \phi(x-2)\frac{\partial\phi(x-5/2)}{\partial x}dx$$

$$-\frac{|\phi(2)|^5}{(\phi(1))^4} \int_{-\infty}^{+\infty} \phi(x-2)\frac{\partial\phi(x-7/2)}{\partial x}dx$$

$$-\frac{|\phi(2)|^6}{(\phi(1))^5} \int_{-\infty}^{+\infty} \phi(x-2)\frac{\partial\phi(x-9/2)}{\partial x}dx \qquad \text{(A12)}$$

and I_2

$$I_2 = |\phi(2)| \int_{-\infty}^{+\infty} \phi(x-3)\frac{\partial\phi(x-1/2)}{\partial x}dx$$

$$+\frac{|\phi(2)|^2}{\phi(1)} \int_{-\infty}^{+\infty} \phi(x-3)\frac{\partial\phi(x-3/2)}{\partial x}dx$$

$$+\frac{|\phi(2)|^3}{(\phi(1))^2} \int_{-\infty}^{+\infty} \phi(x-3)\frac{\partial\phi(x-5/2)}{\partial x}dx$$

$$+\frac{|\phi(2)|^4}{(\phi(1))^3} \int_{-\infty}^{+\infty} \phi(x-3)\frac{\partial\phi(x-7/2)}{\partial x}dx$$

$$+\frac{|\phi(2)|^5}{(\phi(1))^4} \int_{-\infty}^{+\infty} \phi(x-3)\frac{\partial\phi(x-9/2)}{\partial x}dx$$

$$+\frac{|\phi(2)|^6}{(\phi(1))^5} \int_{-\infty}^{+\infty} \phi(x-3)\frac{\partial\phi(x-11/2)}{\partial x}dx. \qquad \text{(A13)}$$

If we take into account the following identity

$$\int_{-\infty}^{+\infty} \phi(x-p)\frac{\partial\phi(x-q)}{\partial x}dx = \int_{-\infty}^{+\infty} \phi(x-p-1)\frac{\partial\phi(x-q-1)}{\partial x}dx, \qquad \text{(A14)}$$

where p, q are any real numbers, then from (A11)-(A12) we conclude that

$$a_{-4} = 0. \qquad \text{(A15)}$$

For the sake of simplicity we verify here the identity (18) only for $i = 1$. All other cases can be checked in the same way. We have

$$a_1 = \int_{-\infty}^{+\infty} Q_{-1}(x)\frac{\partial S_{1/2}(x)}{\partial x}dx = \frac{1}{\phi(1)}\sum_{p=0}^{+\infty}\left(\frac{|\phi(2)|}{\phi(1)}\right)^p$$

$$\cdot \int_{-\infty}^{+\infty} [\phi(x+3)\phi(2)+\phi(x+2)\phi(1)]\frac{\partial\phi_{p-1/2}(x)}{\partial x}dx. \qquad \text{(A16)}$$

If we take into account the support $[0, 3]$ of the Daubechies' scaling function $\phi(x)$ with $N = 2$ then the above equation becomes

$$a_1 = \frac{1}{\phi(1)} \left[I_1 + I_2\right], \tag{A17}$$

where I_1 is given by

$$\begin{aligned}
I_1 &= \phi(2) \int_{-\infty}^{+\infty} \left[\left(\frac{|\phi(2)|}{\phi(1)}\right)^0 \phi(x+3)\frac{\partial\phi(x+1/2)}{\partial x}\right] dx \\
&= -|\phi(2)| \int_{-\infty}^{+\infty} \phi(x+2)\frac{\partial\phi(x-1/2)}{\partial x} dx \tag{A18}
\end{aligned}$$

and I_2

$$\begin{aligned}
I_2 &= \phi(1) \int_{-\infty}^{+\infty} \left[\left(\frac{|\phi(2)|}{\phi(1)}\right)^0 \phi(x+2)\frac{\partial\phi(x+1/2)}{\partial x}\right. \\
&\quad \left. + \left(\frac{|\phi(2)|}{\phi(1)}\right)^1 \phi(x+2)\frac{\phi(x-1/2)}{\partial x}\right] dx \\
&= \phi(1) \int_{-\infty}^{+\infty} \phi(x+2)\frac{\partial\phi(x+1/2)}{\partial x} dx \\
&\quad + |\phi(2)| \int_{-\infty}^{+\infty} \phi(x+2)\frac{\partial\phi(x-1/2)}{\partial x} dx. \tag{A19}
\end{aligned}$$

Finally we combine (A17)–(A19) to obtain

$$\begin{aligned}
a_1 &= \frac{1}{\phi(1)} \left[I_1 + I_2\right] \\
&= \int_{-\infty}^{\infty} \phi(x+2)\frac{\partial\phi(x+1/2)}{\partial x} dx \\
&= \int_{-\infty}^{\infty} \phi(x+1)\frac{\partial\phi(x-1/2)}{\partial x} dx \\
&= \int_{-\infty}^{+\infty} \phi_{-1}(x)\frac{\partial\phi_{1/2}(x)}{\partial x} dx. \tag{A20}
\end{aligned}$$

The last integral in (A20) is exactly equal to a_i given by (2).

REFERENCES

1. Krumpholz, M. and L.P.B. Katehi, "MRTD: New time-domain schemes based on multiresolution analysis," *IEEE Trans. Microwave Theory Tech.*, Vol. 44, 555–571, 1996.

2. Yee, K.S., "Numerical solution of initial boundary value problems involving Maxwell's equation in isotropic media," *IEEE Trans. Antennas Propagat.*, Vol. 14, 302–307, 1996.

3. Cheong, Y. W., Y. M. Less, K. H. Ra, J. G. Kang, and C. C. Shin, "Wavelet-Galerkin scheme of time-dependent inhomogeneous electromagnetic problems," *IEEE Microwave Guided Wave Lett.*, Vol. 9, 297–299, 1999.

4. Daubechies, I., *Ten Lectures on Wavelets*, SIAM, 1992.

5. Sweldens, W. and R. Piessens, "Wavelet sampling techniques," *Proc. Statistical Computing Section*, 20–29, 1993.

6. Walter, G. G., *Wavelets and Other Orthogonal Systems with Applications*, CRC Press, 1994.

7. Tentzeris, E. M., R. L. Robertson, M. Krumpholz, and L. P. B. Katehi, "Application of MRTD to printed transmission lines," *Proc. Microwave Theory Tech. Soc.*, 573–576, 1996.

8. Sheen, D. M., S. M. Ali, M. D. Abouzahra, and J. A. Kong, "Application of the three-dimensional finite-difference time-domain method to the analysis of planar microstrip circuits," *IEEE Trans. Microwave Theory Tech.*, Vol. 38, 849–857, 1990.

9. Tentzeris, E. M., R. L. Robertson, J. F. Harvey, and L. P. B. Katehi, "PML absorbing boundary conditions for the characterization of open microwave circuits using multiresolution time-domain techniques (MRTD)," *IEEE Trans. Antenna Propagat.*, Vol. 47, 1709–1715, 1999.

Youri Tretiakov received the B.Sc. and M.Sc. degrees in electrical engineering, from Moscow Institute of Physics and Technology, Russia, in 1995 and 1997, and the Ph.D. degree in electrical engineering from Arizona State University in 2001. From 1997 to 1998, he worked as a Research Assistant at the Department of Electronic and Electrical Engineering, Trinity College, Ireland. From 1998 to 2001, he was a Research Associate at the Department of Electrical Engineering, Arizona State University. Since 2001 he has been an Advisory Engineer/Scientist with IBM Microelectronics in Burlington, Vermont. His research interests include electromagnetic modeling, CAD tool development for microelectronics, and related areas.

Stanislav Ogurtsov received the diploma degree in physics from Novosibirsk State University in 1993. In 1997 he joined the Department of Applied Electromagnetics, Siberian State University of Telecommunications and Informatics, Novosibirsk, Russia as a

Research and Teaching Associate. From September 2001 until May 2002, he was a Research Visitor at the Electronic Packaging Lab, Arizona State University. Since August 2002 he is a Ph.D. student at Department of Electrical Engineering and Graduate Research Associate at the Electronic Packaging Lab of the Arizona State University.

George W. Pan received the M.S. and Ph.D. degrees in electrical engineering from the University of Kansas, Lawrence, in 1982 and 1984. respectively. From 1984 to 1985, he was a Postdoctoral Fellow at the University of Texas; from 1985 to 1986, he was an Engineer at the Mayo Foundation, Minnesota; from 1986 to 1988, he was an Associate professor at South Dakota State University; and from 1988 to 1995, he was with the University of Wisconsin-Milwaukee, where he was promoted to Professor in 1993. In 1995, he joined Arizona State University, Tempe, as Professor and Director, Electronic Packaging Laboratory of the Electrical Engineering Department. His research area is in applied electromagnetics, packaging, interconnects, and device modeling.